



Title	Superhydrophobic hierarchical surfaces fabricated by anodizing of oblique angle deposited Al–Nb alloy columnar films
Author(s)	Fujii, Takashi; Aoki, Yoshitaka; Habazaki, Hiroki
Citation	Applied Surface Science, 257(19), 8282-8288 <a href="https://doi.org/10.1016/j.apsusc.2011.01.044">https://doi.org/10.1016/j.apsusc.2011.01.044</a>
Issue Date	2011-07-15
Doc URL	<a href="http://hdl.handle.net/2115/47413">http://hdl.handle.net/2115/47413</a>
Type	article (author version)
File Information	ASS257_8282-8288.pdf



[Instructions for use](#)

# **Superhydrophobic Surfaces Fabricated by Oblique Angle Deposition and Anodizing**

Takashi Fujii<sup>1</sup>, Yoshitaka Aoki<sup>1</sup>, Hiroki Habazaki<sup>1,\*</sup>

<sup>1</sup>Division of Materials Chemistry, Faculty of Engineering, Hokkaido University, Sapporo

060-8628, Japan

\*Corresponding author; Phone & Fax: +81-11-706-6575, e-mail:

habazaki@eng.hokudai.ac.jp

## **Abstract**

A combined process of oblique angle magnetron sputtering and anodizing has been developed to tailor superhydrophobic surfaces with dual scale porous morphology. Isolated submicron columns of single-phase Al-Nb alloys are deposited by magnetron sputtering at several oblique deposition angles on a scalloped substrate surface, with the gaps between columns increasing with an increase in the deposition angle from 70 to 110°. Then, the columnar films have been anodized in hot phosphate-glycerol electrolyte to form a nanoporous anodic oxide layer on each column. Such surfaces with submicron-/nano-porous structure have been coated

with a fluoroalkyl phosphate layer to reduce the surface energy. The porous surface before coating is superhydrophilic with a contact angle for water is less than  $10^\circ$ , while after coating the contact angles are larger than  $150^\circ$ , being superhydrophobic. The beneficial effect of dual-scale porosity to enhance the water repellency is found from the comparison of the contact angles of the submicron columnar films with and without nanoporous oxide layers. The larger submicron gaps between columns are also preferable to increase the water repellency.

**Keywords:** sputter deposition, oblique angle deposition, anodizing, dual scale pore structure, superhydrophobic

## 1. Introduction

Physical vapor deposition (PVD), including magnetron sputtering, is a well known technique for the preparation of non-equilibrium, single-phase alloys in a wide composition range [1]. The PVD technique has been generally used to form thin films with flat surfaces, but porous deposits are now available using advanced PVD processes. For instance, porous deposits can be obtained by introducing a flux of depositing atoms at an oblique angle, due to an enhanced self-shadowing effect [2]. Thus, columnar films with open pores are developed.

Combining of controlled substrate rotation with oblique angle deposition (OAD) has also attracted recent attention due to evolution of specific morphologies, such as nanopillars [3, 4] and nanospirals [5, 6]. The use of substrates with periodic surface roughness is also help to tailor the porous films with controlled morphologies [3, 7, 8]. Thus, oblique angle deposition is of considerable interest for the fabrication of nano-engineered film materials.

The authors have recently reported the formation of porous Al-Nb alloy films by oblique angle deposition on scalloped aluminum surfaces [9]. It has been found that the alloy composition of the deposits and their deposition angle change markedly the morphology of deposits. Modification of high surface diffusivity of aluminum adatoms by alloying with niobium during deposition appears to influence the film morphology. At high deposition angle, the Al-36 at% Nb alloy formed a unique nanoplate array film. In this work, such Al-Nb alloy deposits with unique porous morphologies have been used to control the surface wettability.

It is well known that surface wettability is controlled by a chemical factor of solid surface and its surface geometry. Highly water-repellent surfaces can be achieved by reducing the surface energy of solid surface and by introducing the highly porous nature in surface. Wenzel [10] and Cassie-Baxter [11] theories are often cited to correlate the contact angles for water to the roughness of solid surface. There are many examples of superhydrophobic surfaces in nature, such as lotus leaf, water strider legs and cicada wings. Understanding the

complementary roles of surface energy and roughness on the natural water-repellent surfaces has led to the fabrication of a number of biomimetic superhydrophobic surfaces that exhibit apparent contact angles for water greater than  $150^\circ$  [12]. Through these studies, it is now obvious that micro-/nano-dual or multi-scale surface structure is of particular importance for superhydrophobicity [13-18], although the role of such hierarchical surface structure on surface wettability is still unclear [19].

In the present study, the dual scale surface structure has been introduced by a combined process of oblique angle deposition and anodizing (Fig. 1). Porous columnar Al-Nb alloy films prepared by OAD have been anodized to form a nanoporous oxide layer on each alloy column, such that submicron-/nano-dual scale roughness is introduced. Then, the oxide surface has been coated with a fluoroalkyl phosphate (FAP) layer to reduce the surface energy. The resultant surfaces have shown superhydrophobicity. The magnetron-sputtered Al-Nb alloys consist of an amorphous single phase. The single phase materials are necessary to form a nanoporous anodic oxide film uniformly on the entire surface.

## **2. Experimental details**

Columnar Al-Nb films were formed by using DC magnetron sputtering at oblique angles of  $70^\circ$ ,  $85^\circ$ ,  $95^\circ$  and  $110^\circ$ , with respect to substrate normal, on the substrate with a

scalloped surface or at a deposition angle of  $0^\circ$  on a flat glass substrate for 1.8 ks as in our previous report [9]. The alloy compositions changed from 53 at% Nb to 36 at% Nb by increasing the deposition angle from  $0^\circ$  to  $110^\circ$ . All the deposits were amorphous as confirmed by X-ray diffraction measurements. The average thickness of the deposited film and the deposition rate at each deposition angle are summarized in Table 1. The scalloped aluminum substrate was prepared by anodizing 99.99% pure aluminum sheet in  $0.1 \text{ mol dm}^{-3}$  phosphoric acid solution at a constant voltage of 170 V at 293 K for 3.6 ks and subsequent dissolution of the resultant anodic oxide films in a mixture of chromic acid and phosphoric acid at 343 K. During anodizing, self-ordered nanoporous anodic alumina films with hexagonal cell structure were developed [20]. The cell size increases almost linearly with formation voltage [21]. The resultant surface has a cellular morphology with a cell size of  $\sim 400 \text{ nm}$ , as shown in Fig. 2.

The films formed by OAD were anodized in glycerol electrolyte containing  $0.8 \text{ mol dm}^{-3} \text{ K}_2\text{HPO}_4$  at a constant voltage of 10 V at 433 K for 300 s, and then immersed in the same electrolyte for pore-widening of a resultant nanoporous anodic oxide layer. The deposited films before and after anodizing were immersed in ethanol solution containing 2wt% mono-[2-(perfluorooctyl)ethyl]phosphate,  $(\text{CF}_3(\text{CF}_2)_7\text{CH}_2\text{CH}_2\text{OPO}(\text{OH})_2)$ , (FAP) for 5 days at room temperature to cover the surfaces with a monolayer of FAP. FAP was synthesized in the procedure reported previously [22]. The wettability of the specimens obtained was

evaluated by contact angle measurements of a water droplet (2  $\mu\text{L}$ ) using an optical contact angle meter (Kyowa Interface Science Co., DM-CE1). Surfaces and cross-sections of the specimens were observed by a JEOL JSM-6500F field emission scanning electron microscope (SEM).

## Results and Discussion

Fig. 3 shows surface and cross-sectional SEM images of the porous anodic oxide layer formed on the flat Al-Nb alloy film sputter-deposited on a flat glass substrate.

Obviously, a porous layer of  $\sim 200$  nm thickness is developed on the alloy film. The pore size is as small as  $\sim 10$  nm and the interpore distance is about 30 nm. The formation of the porous anodic layer of such small pores is characteristic of the electrolyte used, and the formation of porous anodic layer of similar pore structure has been reported on aluminum [23, 24], titanium [25] and niobium [26, 27].

Fig. 4 shows surface and cross-sectional SEM images of the sputter-deposited columnar Al-Nb films formed at several oblique angles on a scalloped substrate with a cell size of about 400 nm. Cross-sectional images (Figs. 4(e)-(h)) disclose the development of columns tilted to the incident direction. The columns are isolated and developed mainly on the ridge regions (triple points) of the substrate (Fig. 2), such that a hexagonal array of

columns is seen from the surface images (Figs. 4(a)-(d)). In addition, the shape of columns changes from round-type at a deposition angle of  $70^\circ$ , through square- or triangle-type at  $85^\circ$  and  $95^\circ$ , to apparent plate-type at  $110^\circ$ , and the top of columns tends to sharpen at higher deposition angles. The column width increases as the distance from the substrate increases, when the deposition angle is  $70^\circ$ , while the width becomes almost constant in column length direction at the deposition angle of  $85^\circ$ . Further increase in the deposition angle results in narrowing of the column width to the direction of the top of columns. Thus, the gaps between columns become wider as the deposition angle is increased. From the surface SEM image (Fig. 4(d)), the gaps are apparently  $\sim 250$  nm at the deposition angle of  $110^\circ$ . An enhanced shadow effect at higher deposition angles develops thinner columns, although the film thickness, i.e., column length, also decreases at higher deposition angles.

Anodizing of the isolated columnar films in hot phosphate-glycerol electrolyte results in the formation of a nanoporous anodic layer on each column (Fig. 5). Surface roughening is evident after anodizing, and the pore size of the oxide layer is again  $\sim 10$  nm as in the case of the anodic oxide layer formed on the flat Al-Nb alloy (Fig. 3). From the comparison between Figs. 4 and 5, the gaps between columns are slightly reduced after anodizing, since the thickness of the anodic oxide layer is greater than the thickness of the alloy consumed by anodizing.

The oxide surface is usually hydrophilic, such that the oxide surface has been coated

with a fluoroalkyl layer to change the surface from hydrophilic to hydrophobic. It is known that the maximum contact angle of hydrophobic surfaces for water cannot exceed  $\sim 120^\circ$  when the surface is flat [28]. Thus, the surface roughness must be introduced to change from hydrophobic to superhydrophobic state. In the present study, the flat and porous surfaces were coated with FAP by single immersion of specimens in ethanol solution containing 2 wt% FAP. In ideal case, a monolayer of FAP should cover the entire flat and porous surfaces, but the direct confirmation of the monolayer coating was rather difficult. The coating was performed for various periods of immersion time. The contact angle for water became constant after immersion for 5 days. We assumed the saturated coverage of FAP on surface after this immersion period. The coated specimens thus prepared have been used in the present study for the contact angle measurements for water.

Fig. 6 shows the static water contact angles of various specimens. The contact angle of a water droplet placed on a flat Al-Nb film covered with FAP was  $116.6^\circ$ . Since the surface is flat, the contact angle is less than  $120^\circ$  as discussed above. The columnar alloy film deposited at  $110^\circ$  shows a water contact angle of  $65.7^\circ$  before FAP coating, indicating that the surface is hydrophilic. The contact angle is markedly reduced to less than  $10^\circ$  after anodizing. Superhydrophilicity is obtained by introducing the submicron-/nano-dual roughness. The FAP-coated nanoporous anodic oxide layer formed on the flat Al-Nb alloy film shows a contact angle of  $127.6^\circ$ , which is larger than that on the coated flat surface. The enhanced

water repellency is more obvious when the isolated columnar Al-Nb film is coated with FAP. The contact angle larger than  $150^\circ$  is obtained. Further slight increase in the contact angle occurs when the anodized columnar film is coated with FAP. In addition to the increased static contact angle, it was found that the water droplet rolled off more readily on the dual-scale porous surface. Thus, both the coated columnar films with and without an anodic oxide layer are superhydrophobic, but the former is more water-repellent.

The importance of the dual-scale pore structure is more obvious for the specimens deposited at lower angles. Fig. 7 shows the water contact angle of the FAP-coated alloy films with and without anodic oxide layers as a function of deposition angle. At the deposition angle of  $70^\circ$ , the contact angle exceeds  $150^\circ$  only when submicron-/nano-porous structure is developed. For both the specimens with and without anodic oxide layers, the contact angle increases with an increase in the deposition angle. The gaps between columns enlarge with the deposition angle (Figs. 4 and 5). As a consequence, the porosity increases and the difference of two pore sizes also increases with the deposition angle. Such situation is preferable for enhancing water repellency.

### **3. Conclusions**

1) Isolated columnar Al-Nb films are formed on a scalloped aluminum substrate with regular

concave cell structure by oblique angle deposition. The column shape and the size of gaps between columns are dependent upon the deposition angle with wider gaps developing at higher deposition angles.

2) Anodizing of the flat and columnar Al-Nb films at 10 V in hot phosphate-glycerol electrolyte forms a nanoporous anodic oxide layer with a pore size of ~10 nm.

3) The anodized Al-Nb columnar films with submicron-/nano-dual scale pores are superhydrophilic. After coating with a fluoroalkyl phosphate layer, the surface becomes superhydrophobic. Although the coated columnar films without nanoporous anodic oxide layers are also superhydrophobic, the dual-scale porous structure further enhances the superhydrophobicity.

## **Acknowledgement**

Thanks are due to Dr. Masanori Yoshida, Division of Chemical Process Engineering, Faculty of Engineering, Hokkaido University, for his help with synthesis of mono-[2-(perfluorooctyl)ethyl] phosphate. The present work was supported in part by Grants-in-Aid for Scientific Research (A) No. 19206077 and for Exploratory Research, No.21656180 from the Japan Society for the Promotion of Science, and also by the Global COE Program (Project No. B01: Catalysis as the Basis for Innovation in Materials Science) from the Ministry of Education, Culture, Sports, Science and Technology, Japan.

## References

- [1] K. Hashimoto, P.Y. Park, J.H. Kim, H. Yoshioka, H. Mitsui, E. Akiyama, H. Habazaki, A. Kawashima, K. Asami, Z. Grzesik, S. Mrowec, Recent Progress in Corrosion-Resistant Metastable Alloys, *Mater. Sci. Eng. A*, 198 (1995) 1-10.
- [2] L. Abelmann, C. Lodder, Oblique evaporation and surface diffusion, *Thin Solid Films*, 305 (1997) 1-21.
- [3] C.M. Zhou, D. Gall, The structure of Ta nanopillars grown by glancing angle deposition, *Thin Solid Films*, 515 (2006) 1223-1227.
- [4] K. Robbie, C. Shafai, M.J. Brett, Thin films with nanometer-scale pillar microstructure, *J. Mater. Res.*, 14 (1999) 3158-3163.
- [5] M. Suzuki, T. Ito, Y. Taga, Photocatalysis of sculptured thin films of TiO<sub>2</sub>, *Appl. Phys. Lett.*, 78 (2001) 3968-3970.
- [6] R. Messier, V.C. Venugopal, P.D. Sunal, Origin and evolution of sculptured thin films, *J. Vac. Sci. Technol., A*, 18 (2000) 1538-1545.
- [7] M.O. Jensen, M.J. Brett, Periodically structured glancing angle deposition thin films, *IEEE Tran. Nanotech.*, 4 (2005) 269-277.
- [8] M.T. Tanvir, K. Fushimi, Y. Aoki, H. Habazaki, Oblique angle deposition of columnar niobium films for capacitor application, *Mater. Trans.*, 49 (2008) 1320-1326.
- [9] T. Fujii, Y. Aoki, K. Fushimi, T. Makino, S. Ono, H. Habazaki, Controlled morphology of aluminum alloy nanopillar films: from nanohorns to nanoplates, *Nanotechnol.*, 21 (2010) 395302.
- [10] R.N. Wenzel, Resistance of solid surfaces to wetting by water, *Ind. Eng. Chem.*, 28 (1936) 988-994.

- [11] A.B.D. Cassie, S. Baxter, Wettability of porous surfaces, *Trans. Faraday Soc.*, 40 (1944) 546-551.
- [12] T.L. Sun, L. Feng, X.F. Gao, L. Jiang, Bioinspired surfaces with special wettability, *Acc. Chem. Res.*, 38 (2005) 644-652.
- [13] N. Zhao, J. Xu, Q.D. Xie, L.H. Weng, X.L. Guo, X.L. Zhang, L.H. Shi, Fabrication of biomimetic superhydrophobic coating with a micro-nano-binary structure, *Macromol. Rapid Commun.*, 26 (2005) 1075-1080.
- [14] M. Nosonovsky, B. Bhushan, Roughness optimization for biomimetic superhydrophobic surfaces, *Microsystem Technol. Micro- and Nanosystems*, 11 (2005) 535-549.
- [15] M. Nosonovsky, Multiscale roughness and stability of superhydrophobic biomimetic interfaces, *Langmuir*, 23 (2007) 3157-3161.
- [16] Y.C. Jung, B. Bhushan, Contact angle, adhesion and friction properties of micro- and nanopatterned polymers for superhydrophobicity, *Nanotechnol.*, 17 (2006) 4970-4980.
- [17] M. Nosonovsky, B. Bhushan, Biomimetic superhydrophobic surfaces: Multiscale approach, *Nano Lett.*, 7 (2007) 2633-2637.
- [18] H.E. Jeong, S.H. Lee, J.K. Kim, K.Y. Suh, Nanoengineered multiscale hierarchical structures with tailored wetting properties, *Langmuir*, 22 (2006) 1640-1645.
- [19] A.H.F. Wu, K.L. Cho, I.I. Liaw, G. Moran, N. Kirby, R.N. Lamb, Hierarchical surfaces: an in situ investigation into nano and micro scale wettability, *Faraday Discuss.*, 146 (2010) 223-232.
- [20] J.P. O'Sullivan, G.C. Wood, Morphology and mechanism of formation of porous anodic films on aluminum, *Proc. R. Soc. London, A*, 317 (1970) 511-543.
- [21] K. Ebihara, H. Takahashi, M. Nagayama, Structure and density of anodic oxide films formed on aluminum in oxalic acid solutions *J. Surf. Finish. Soc. Jpn.*, 35 (1983) 548-553.
- [22] S. Shibuichi, T. Yamamoto, T. Onda, K. Tsujii, Super water- and oil-repellent surfaces

- resulting from fractal structure, *J. Colloid Interface Sci.*, 208 (1998) 287-294.
- [23] Q. Lu, G. Alcala, P. Skeldon, G.E. Thompson, M.J. Graham, D. Mashedier, K. Shimizu, H. Habazaki, Porous tantalum and alumina films from non-thickness limited anodising in phosphate/glycerol electrolyte, *Electrochim. Acta*, 48 (2002) 37-42.
- [24] S. Yang, Y. Aoki, P. Skeldon, G.E. Thompson, H. Habazaki, Growth of porous anodic alumina films in hot phosphate–glycerol electrolyte, *J. Solid State Electrochem.*, (2010) in press.
- [25] H. Habazaki, M. Teraoka, Y. Aoki, P. Skeldon, G.E. Thompson, Formation of porous anodic titanium oxide films in hot phosphate/glycerol electrolyte, *Electrochim. Acta*, 55 (2010) 3939-3943.
- [26] Q. Lu, T. Hashimoto, P. Skeldon, G.E. Thompson, H. Habazaki, K. Shimizu, Nanoporous anodic niobium oxide formed in phosphate/glycerol electrolyte, *Electrochim. Solid State Lett.*, 8 (2005) B17-B20.
- [27] H. Habazaki, Y. Oikawa, K. Fushimi, Y. Aoki, K. Shimizu, P. Skeldon, G.E. Thompson, Importance of water content in formation of porous anodic niobium oxide films in hot phosphate-glycerol electrolyte, *Electrochim. Acta*, 54 (2009) 946-951.
- [28] T. Nishino, M. Meguro, K. Nakamae, M. Matsushita, Y. Ueda, The lowest surface free energy based on  $-CF_3$  alignment, *Langmuir*, 15 (1999) 4321-4323.

## Figure Captions

Figure 1 Schematic illustration showing the fabrication process of water-repellent surfaces. (a) Anodizing of an aluminum sheet in phosphoric acid and subsequent dissolution of the resultant porous oxide layer in  $\text{H}_3\text{PO}_4\text{-CrO}_3$  solution to form the scalloped substrate, (b) magnetron sputter-deposition of Al-Nb alloy columns at oblique angles on the scalloped substrate, (c) anodizing of columnar Al-Nb alloy films in hot phosphate-glycerol electrolyte to form a nanoporous oxide layer on each column, and (d) coating with fluoroalkyl phosphate to reduce surface energy.

Figure 2 Atomic force microscope image of the scalloped aluminum substrate surface; (a) 3D view and (b) cross-sectional view at the line in (a).

Figure 3 (a) Surface and (b) cross-sectional scanning electron micrographs of the Al-53 at% Nb alloy film deposited on flat glass substrate after anodizing in  $0.8 \text{ mol dm}^{-3} \text{ K}_2\text{HPO}_4\text{-glycerol}$  electrolyte at a constant voltage of 10 V for 300 s at 433 K, and then immersed in the same electrolyte for 600 s.

Figure 4 Scanning electron micrographs of ((a)-(d)) surfaces and ((e)-(h)) cross-sections of the Al-Nb alloy films deposited at oblique angles of ((a), (e))  $70^\circ$ , ((b), (f))  $85^\circ$ , ((c), (g))  $95^\circ$  and ((d), (h))  $110^\circ$  on scalloped aluminum substrate for 1.8 ks.

Figure 5 Scanning electron micrographs of ((a)-(d)) surfaces and ((e)-(h))

cross-sections of the Al-Nb alloy films deposited at oblique angles of ((a), (e)) 70°, ((b), (f)) 85°, ((c), (g)) 95° and ((d), (h)) 110° on scalloped aluminum substrate for 1.8 ks, followed by anodizing in 0.8 mol dm<sup>-3</sup> K<sub>2</sub>HPO<sub>4</sub>-glycerol electrolyte at a constant voltage of 10 V for 0.3 ks at 433 K and subsequent immersion in the same electrolyte for 600 s.

Figure 6            Static contact angles of a water droplet placed on FAP-coated flat Al-Nb alloy surface, non-coated columnar films with and without a nanoporous oxide layer, dual scale porous film, FAP-coated single nanoporous oxide film, FAP-coated columnar film with and without a nanoporous anodic oxide layer. The columnar Al-Nb alloy film was deposited at an oblique angle of 110°.

Figure 7            Static contact angles of the FAP-coated surfaces with dual scale pores (○) and single submicron pores (□) as a function of deposition angle in OAD.

Table 1 Thicknesses and average deposition rates of the Al-Nb alloys sputter-deposited at several oblique angles on a scalloped aluminum substrate for 1.8 ks.

Deposition angle (deg.)	Film thickness (nm)	Deposition rate (nm s <sup>-1</sup> )
70	810	0.45
85	700	0.39
95	540	0.30
110	440	0.24

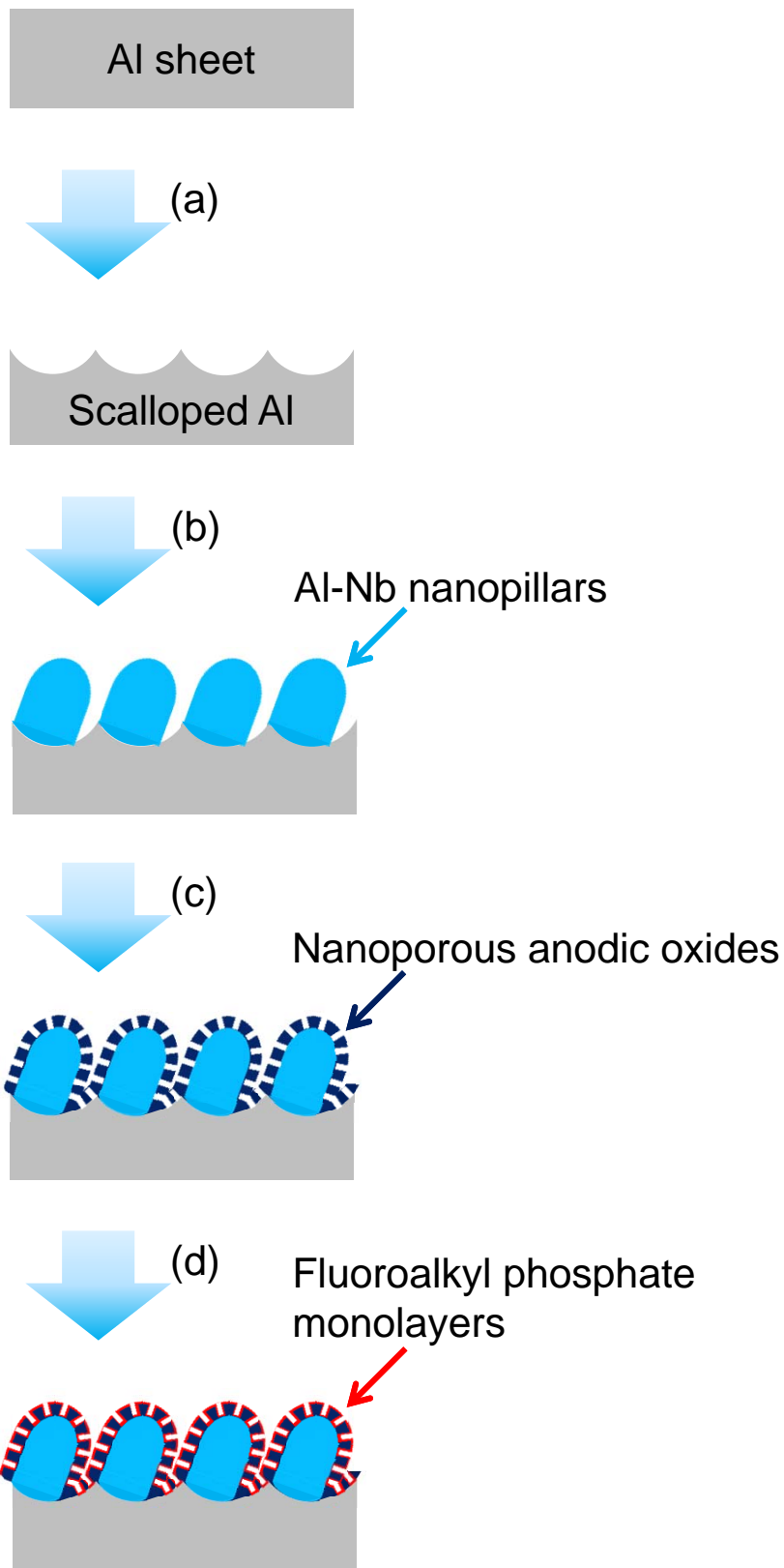
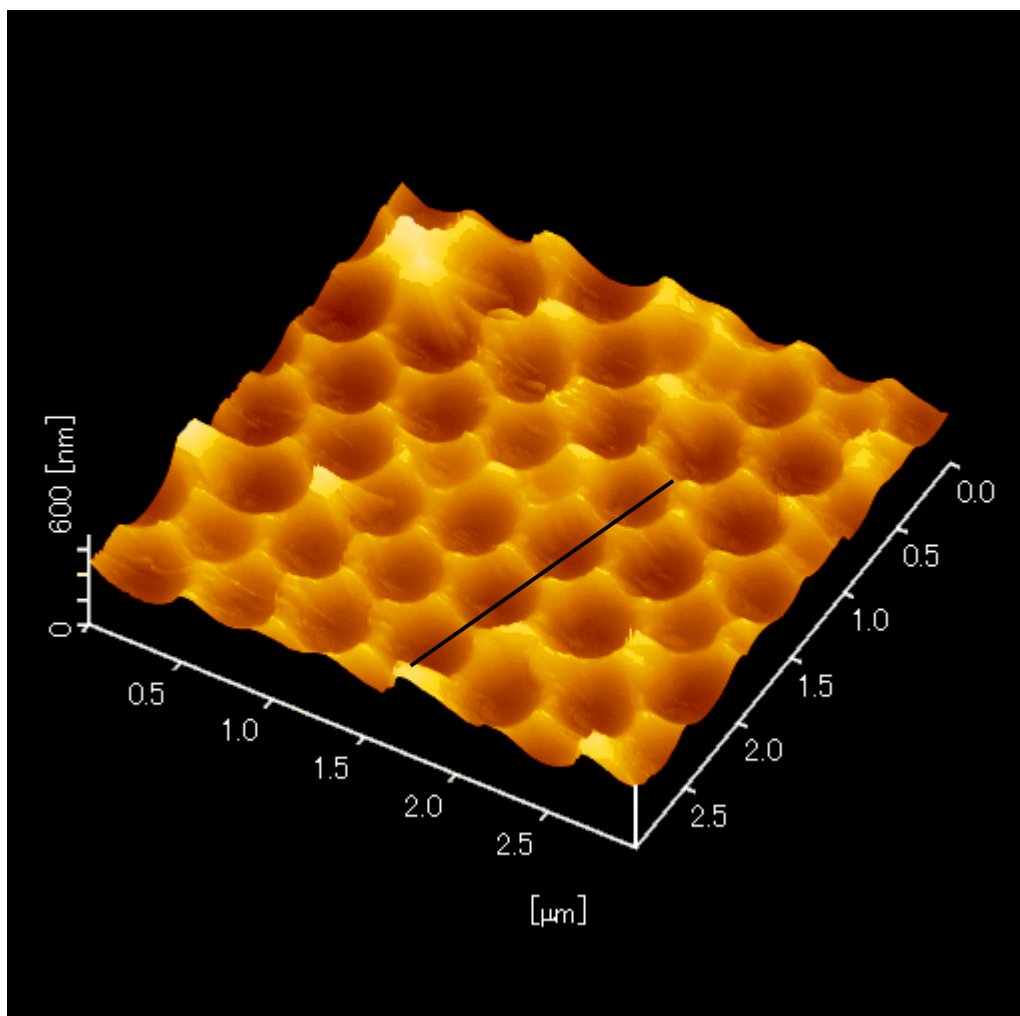


Figure 1

(a)



(b)

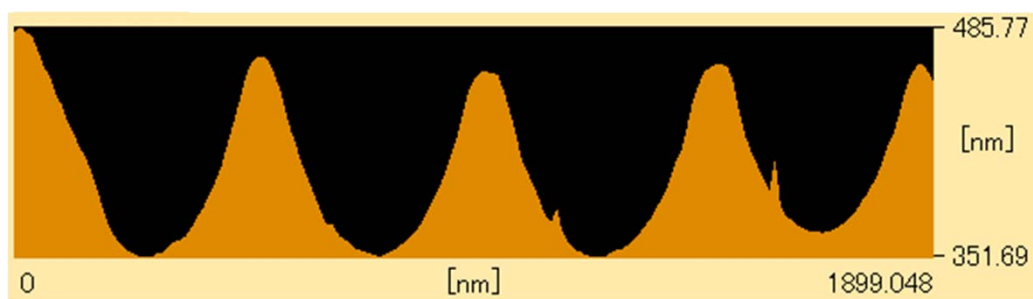


Figure 2

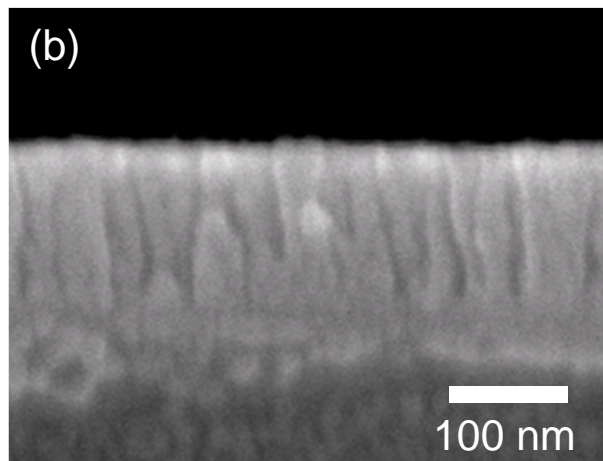
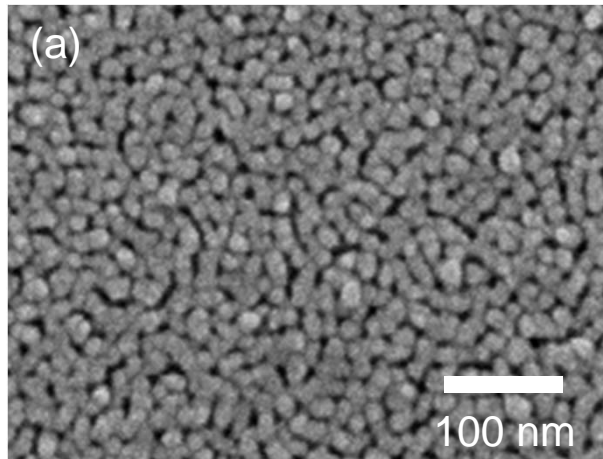


Figure 3

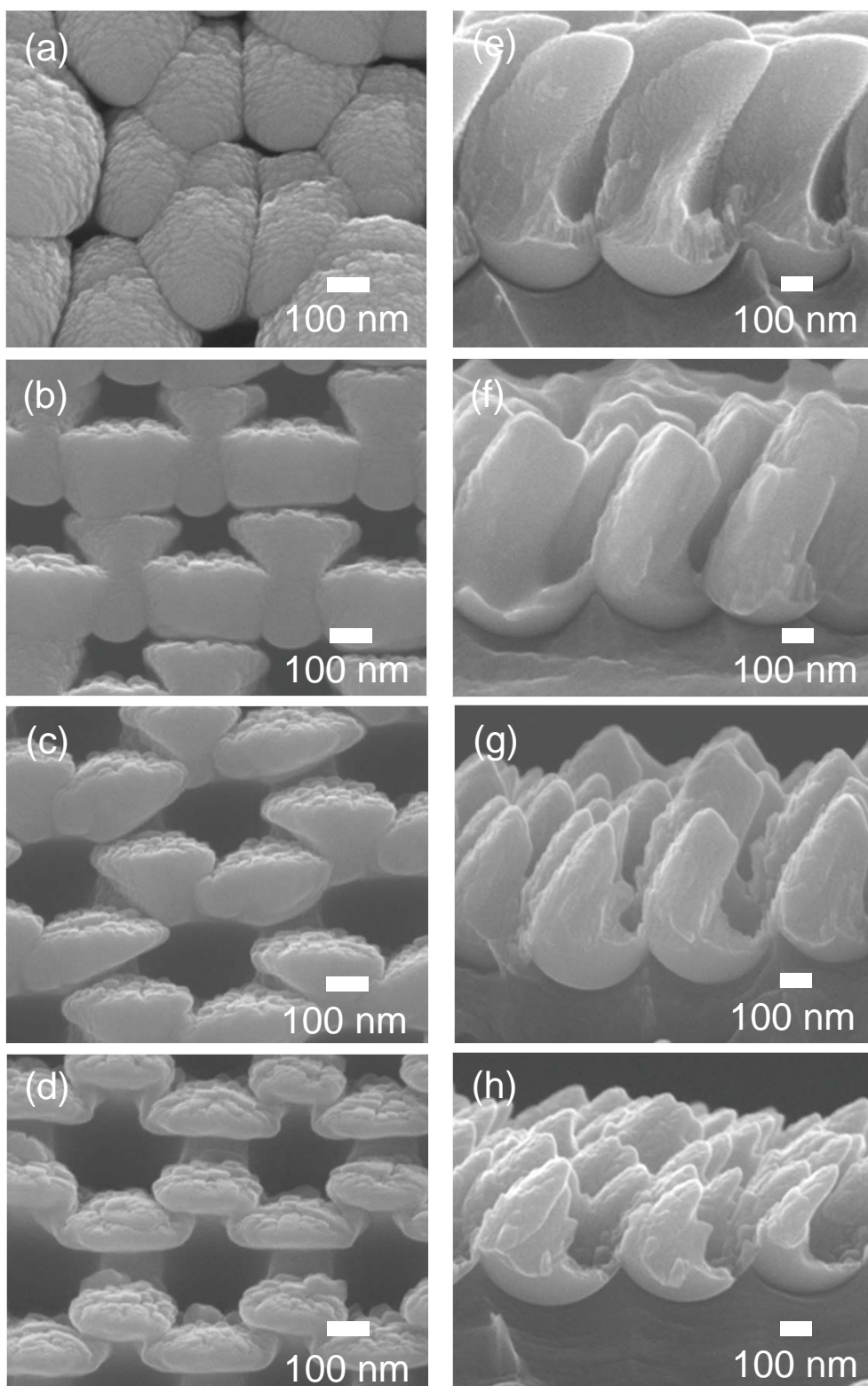


Figure 4

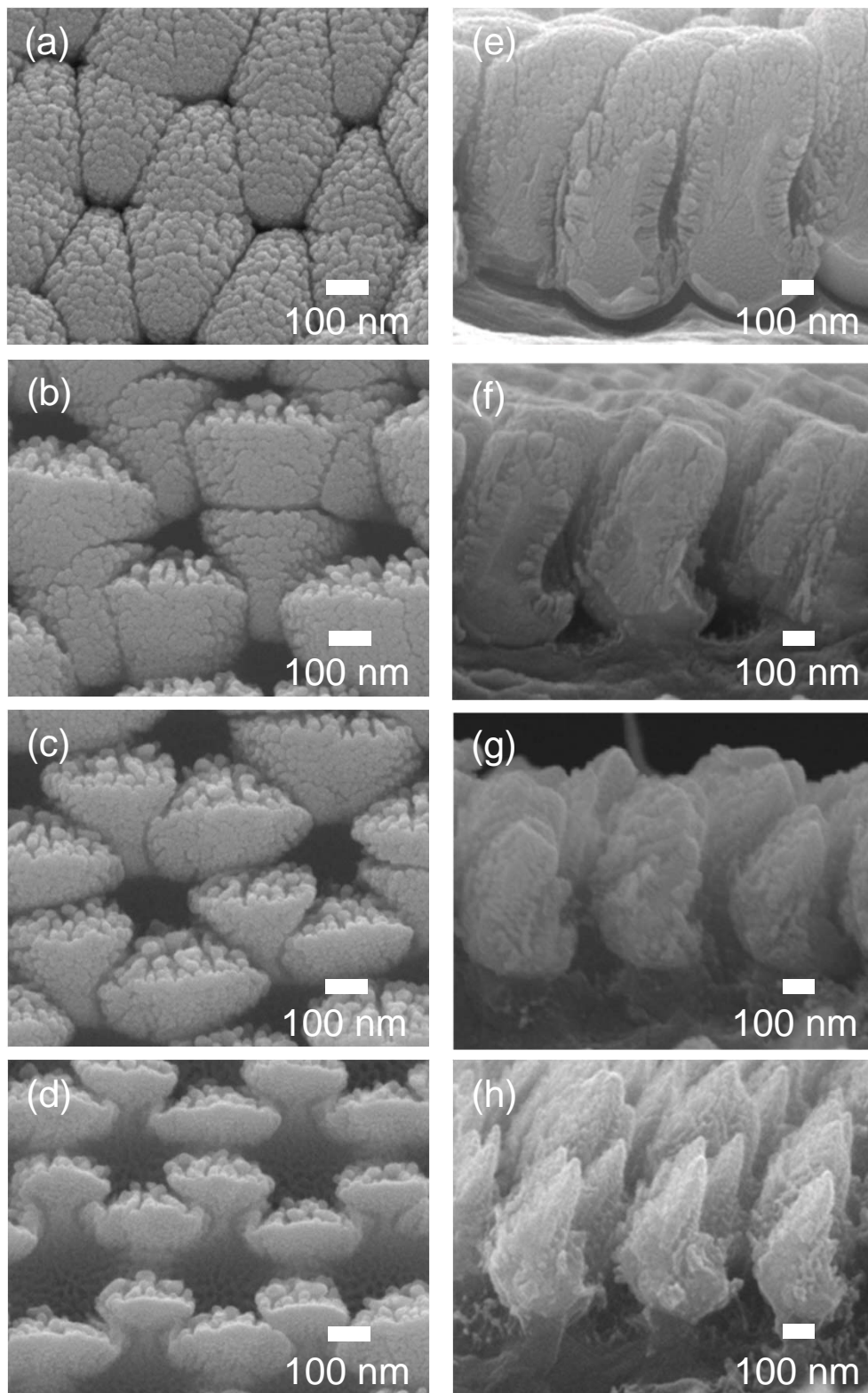


Figure 5

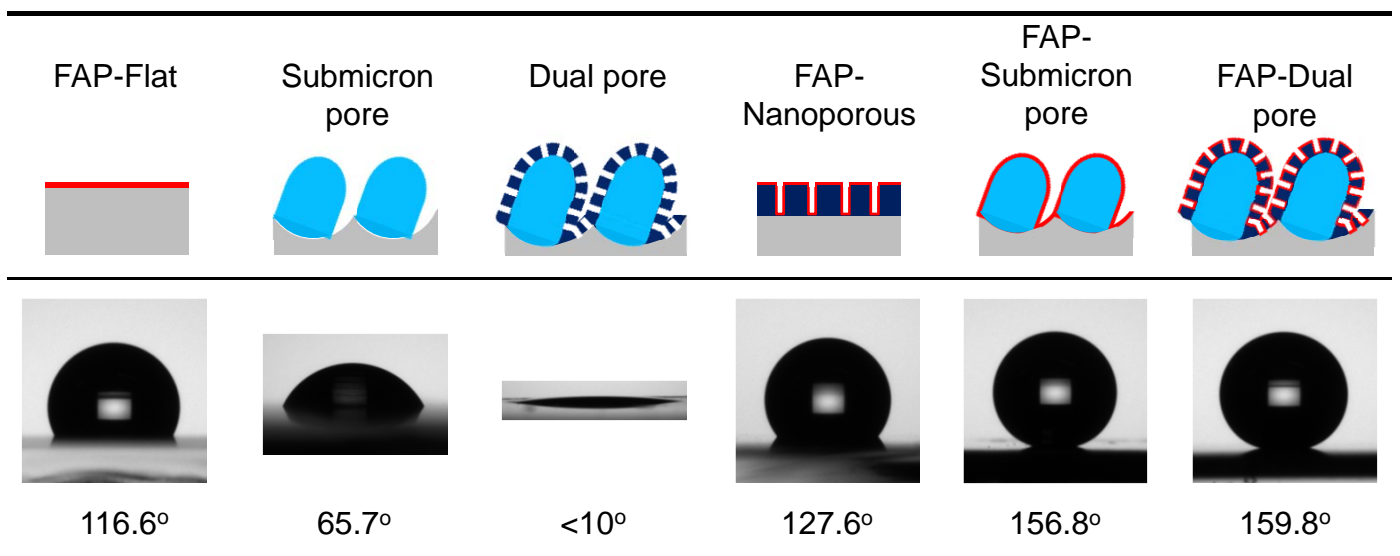


Figure 6

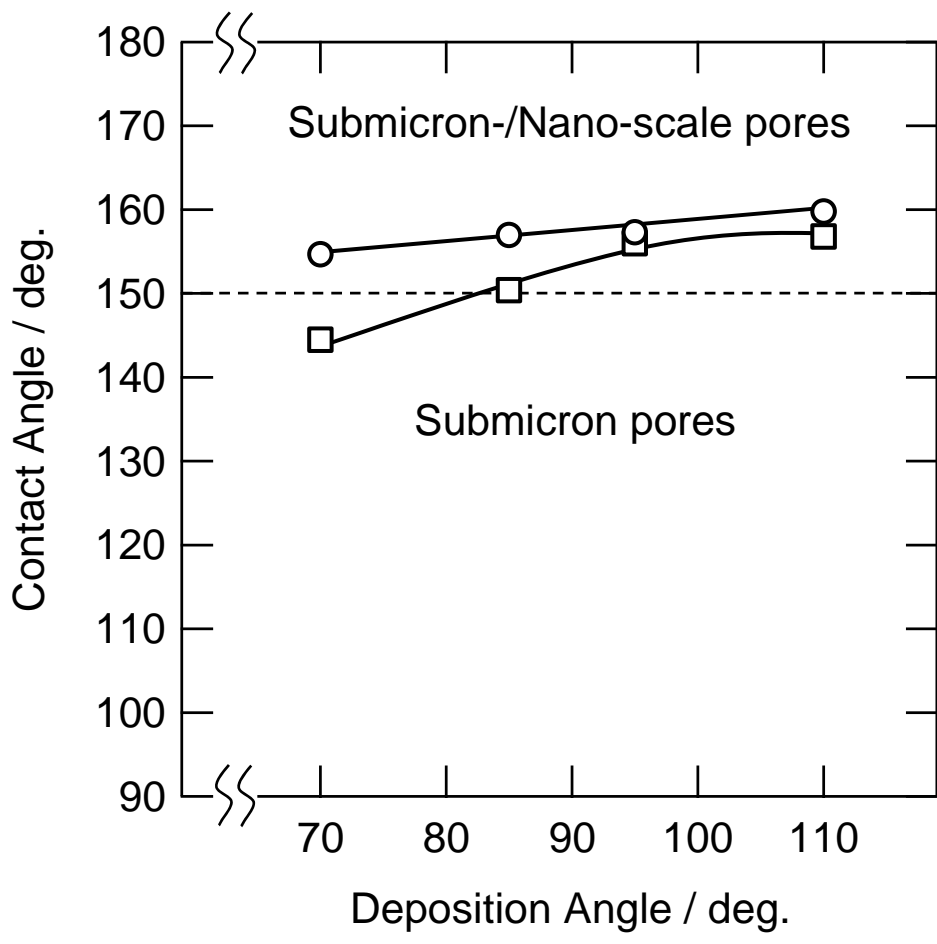


Figure 7